Brownian Dynamics Simulation of Biased Sinusoidal Field Gel Electrophoresis†

Yuichi Masubuchi, Hidehiro Oana, Mitsuhiro Matsumoto, and Masao Doi*

School of Engineering, Nagoya University, Nagoya 464-01, Japan

Received August 22, 1996; Revised Manuscript Received November 4, 1996⊗

ABSTRACT: Brownian dynamics simulation of DNA in the biased sinusoidal field gel electrophoresis was performed. The time development of the velocity of the center of mass and the principal value of the gyration tensor was measured as a function of the chain length and the frequency of the applied field. It is found that (i) for short chains $N < N_c$(E), the mean migration velocity decreases monotonically with the frequency, and that (ii) for long chains $N > N_c(E)$, the mean migration velocity shows local minimum and local maximum at characteristic frequencies f_1 and f_2, respectively. These results are in agreement with the experiment of Shikata et al. Analysis of the data indicates that the DNA takes the stretched V-conformation and compact conformation alternatively, while at the frequency f_1 the DNA frequently takes the W-conformation.

1. Introduction

Gel electrophoresis is a technique widely used to separate DNA molecules according to their length. However the physics underlying the technique is not well-understood.[1,2] Under the usual experimental condition, the mean migration velocity is a nonlinear function of the applied field. If the applied field is time dependent, the migration velocity shows a rather complex behavior.

Carle et al.,[3] Heller and Pohl,[4] and Kobayashi et al.[5] investigated the mobility of oligomers of λ DNA and yeast chromosomes during field inversion gel electrophoresis (FIGE) in which the field is varied as

$$E(t) = \begin{cases} E_0 & nT < t < nT + t_1 \\ -E_0 & nT + t_1 < t < (n+1)T \end{cases} \quad (1)$$

where n is an integer, t_1 is the duration time of the forward pulse, and T is the periodicity. They found that the mobility takes a minimum at a certain pulse time which depends on the molecular weight of DNA. This phenomenon is called the antiresonance.

Similar phenomenon has been observed by Shikata et al.[6] who studied the mobility for biased sinusoidal field gel electrophoresis (BSFGE) in which the field is varied as $E(t) = E_b + E_s \sin 2\pi ft$. Their result is shown in Figure 1. The mobility of small DNA (less than 10 kbp) decreases monotonically with the increase of the frequency. On the other hand, the mobility of large DNA shows a local minimum and a local maximum as a function of the frequency. The local minimum corresponds to the antiresonance found in the FIGE.

A clue to understand this mysterious phenomenon was given by the study of the conformational dynamics of DNA in steady field gel electrophoresis.[7,8] Fluorescence microscopy[9,10] and computer simulation[11] showed that in steady field gel electrophoresis, large DNA migrates with a stretch−contraction motion each characterized by the V-conformation and a spherical coil conformation, respectively. The conformational change

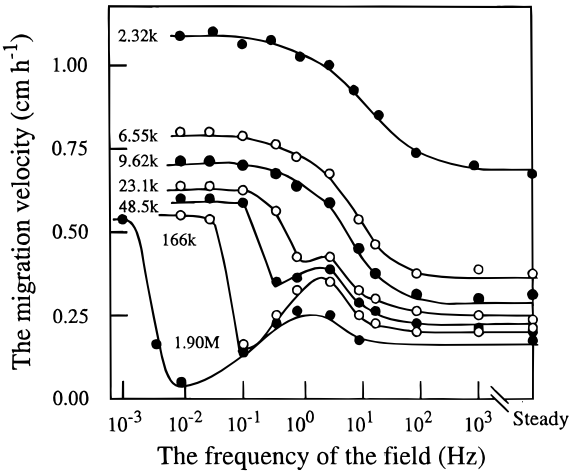

Figure 1. The migration velocity of DNA fragments during BSFGE.[6] Molecular weight is indicated on the left end of each line. Other experimental conditions are follows: 1.0 wt %, agarose gel, 50 mM TBE buffer, 20 °C, the field parameter E_b = 2.5V/cm and E_s = 7.5V/cm.

is periodic and the period is close to the field switching time when the antiresonance occurs.[12−14] This suggests that the antiresonance is caused by some coupling of the field switching and the conformational change of DNA. However, the detail of the nature of the coupling is not known.

In order to understand the conformational dynamics of DNA in gel electrophoresis, we have been performing a computer simulation and direct observation of DNA during BSFGE. In the earlier work,[15] we have shown that in the antiresonance condition DNA motion is hindered by several competitive kinks coexisting on DNA: DNA frequently takes the W-conformation instead of the V-conformation. In this study, however, the molecular weight of DNA was fixed. In this paper, we report on the molecular weight dependence of the conformational change of DNA during BSFGE. We shall demonstrate that the computer simulation give results in good agreement with experiments. By the computer simulation, we can study the conformational change in detail and we shall propose a picture of DNA motion during BSFGE.

2. Model

2.1. Equation of Motion. The model used in the computer simulation is the same as that in ref 15 and

† Abbreviations: BSFGE, biased sinusoidal field gel electrophoresis; FIGE, field inversion gel electrophoresis; kbp, kilobase-pairs; PFGE, pulsed field gel electrophoresis.

* To whom correspondence should be addressed. Phone: 81-52-789-3718. FAX: 81-52-789-3724. E-Mail doi@nuap.nagoya-u.ac.jp.

⊗ Abstract published in *Advance ACS Abstracts,* January 1, 1997.

S0024-9297(96)01273-9 CCC: $14.00

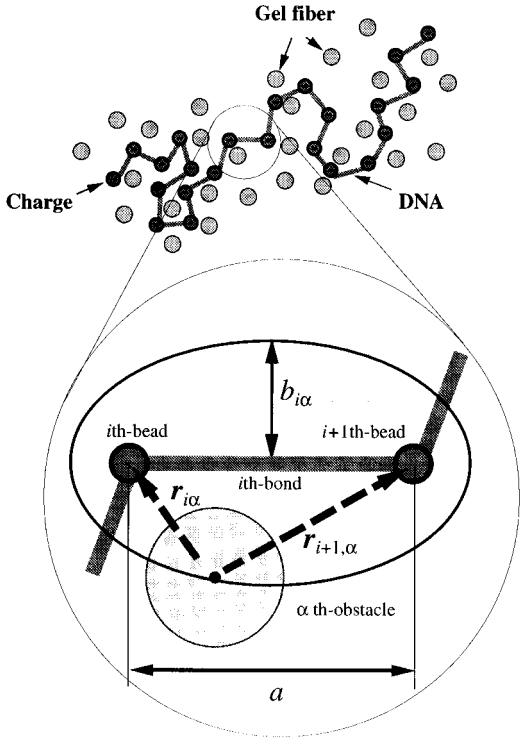

Figure 2. The model of the computer simulation and a schematic representation of the repulsive potential $U_{i\alpha}^{\text{bond}}$.

is schematically represented in Figure 2. The DNA molecule is modeled by a chain composed of N beads, each having charge q and friction constant ζ, connected by bonds of constant length a. The DNA is placed in a two dimensional plane. The gel is modeled by a set of rigid fibers which are standing perpendicularly to the plane. The circles in Figure 2 denote the cross section of the fibers across which the DNA cannot move. The circles are called obstacles. The position of the i -th bead, $\boldsymbol{r}_i$, obeys the following Langevin equation:[11,16,17]

$$\zeta \dot{\boldsymbol{r}}_i = q\boldsymbol{E} - \frac{\partial U^{\text{gel}}}{\partial \boldsymbol{r}_i} + \boldsymbol{f}_i + \lambda_i(\boldsymbol{r}_{i+1} - \boldsymbol{r}_i) - \lambda_{i-1}(\boldsymbol{r}_i - \boldsymbol{r}_{i-1}) \tag{2}$$

The right hand side of eq 2 represents various forces acting on the bead:

(1) $q\boldsymbol{E}$ represents the force of the electric field.

(2) $-\partial U^{\text{gel}}/\partial \boldsymbol{r}_i$ represents the force exerted by the obstacles. The force is introduced to prevent the chain crossing the obstacles. The actual form of the potential U^{gel} is given later.

(3) $\boldsymbol{f}_i$ represents the random force due to the thermal fluctuations of the solvent molecules. It is generated at every time step according to the Gaussian distribution characterized by the following moments.

$$\langle \boldsymbol{f}_i \rangle = 0 \tag{3}$$

$$\langle \boldsymbol{f}_i(t)\, \boldsymbol{f}_j(t') \rangle = 2k_{\text{B}}T\zeta\delta_{ij}\mathbf{I}\delta(t - t') \tag{4}$$

(4) $\lambda_i(\boldsymbol{r}_{i+1} - \boldsymbol{r}_i)$ and $\lambda_{i-1}(\boldsymbol{r}_i - \boldsymbol{r}_{i-1})$ represent the force exerted by the neighboring beads, where $\{\lambda_i\}$ are the Lagrange multipliers which are determined in every time step to keep the bond length constant: For given $\{\boldsymbol{r}_i\}$ and $\{\boldsymbol{f}_i\}$, $\{\boldsymbol{r}_i(t + \delta t)\}$ are determined by $\{\boldsymbol{r}_i(t + \delta t) = \boldsymbol{r}_i(t) + \dot{\boldsymbol{r}}_i\delta t\}$ and $\{\lambda_i\}$ are determined by the constraint $\{(\boldsymbol{r}_{i+1}(t + \delta t) - \boldsymbol{r}_i(t + \delta t))^2 = a^2\}$.

2.2. The Potential. The potential U^{gel} represents the interaction between the chain and the obstacles. The role of the potential is to prevent the chain from crossing the obstacles. In the earlier works,[11,16,17] this was attained by a repulsive potential acting between the obstacles and the *beads*. In such a model, however, one has to assume a rather large range of repulsion (larger than half of the bond length) in order to ensure the noncrossability of the chain across the obstacles. Such a model corresponds to a "fat" chain, where the diameter of the chain is nearly the same as the bond length of DNA. In order to perform a simulation for a "thin" chain, we used the model that the interaction potential is a sum of the interaction between the obstacles and the *bonds*.

$$U^{\text{gel}} = \sum_i \sum_\alpha U_{i\alpha}^{\text{bond}} \tag{5}$$

where $U_{i\alpha}^{\text{bond}}$ is the repulsive potential between bond i and obstacle α. This is determined as follows (see Figure 2). We consider an ellipse $D_{i\alpha}$ which is determined by the bond i and obstacle α: The foci of $D_{i\alpha}$ is located at both ends of the bond i, i.e, at the beads i and $i + 1$, and $D_{i\alpha}$ passes the center of the obstacle α. We assume that $U_{i\alpha}^{\text{bond}}$ depends on the length of its shorter principal axis, $b_{i\alpha}$, as

$$U_{i\alpha}^{\text{bond}} = k_{\text{B}}T(\sigma/b_{i\alpha})^6 \tag{6}$$

where σ is a parameter. Since $b_{i\alpha}$ approaches zero as the bond i comes close to the center of the obstacle α, the potential of eq 6 prevents the bond i from crossing the obstacle α. The length $b_{i\alpha}$ is determined by the position vectors $\boldsymbol{r}_{i\alpha}$ and $\boldsymbol{r}_{i+1\alpha}$ of the bead i and $i + 1$ relative to the position of the obstacle α. It can be shown that

$$b_{i\alpha} = \frac{1}{2}[(|\boldsymbol{r}_{i+1\alpha}| + |\boldsymbol{r}_{i\alpha}|)^2 - |\boldsymbol{r}_{i\alpha} - \boldsymbol{r}_{i+1\alpha}|^2]^{1/2} \tag{7}$$

Although the potential of eq 5 is sufficient to prevent the bond crossing, we added another term to U^{gel} in order to make the equipotential surface of U^{gel} smooth. The added term consists of the interaction between the obstacles and the *beads*, and is written as

$$U_{i\alpha}^{\text{bead}} = k_{\text{B}}T(\sigma/|\boldsymbol{r}_{i\alpha}|)^6 \tag{8}$$

Consequently, the total interaction potential is written as

$$U^{\text{gel}} = \sum_i \sum_\alpha U_{i\alpha}^{\text{bead}} + \sum_i \sum_\alpha U_{i\alpha}^{\text{bond}} \tag{9}$$

The parameter σ in eqs 6 and 8 determines the size of the obstacles. We fixed σ at $\sigma = 0.25a$. This is chosen so that $U_{i\alpha}^{\text{bead}}$ is equal to $k_{\text{B}}T$ when $|\boldsymbol{r}_{i\alpha}| = 0.25a$.

2.3. Parameters. We chose a as the unit of length, $k_{\text{B}}T$ as the unit of energy, and $\zeta a^2/k_{\text{B}}T$ as the unit of time. In this scale, the electric field is represented by a dimensionless quantity,

$$\Theta = \frac{qEa}{k_{\text{B}}T} \tag{10}$$

We used the following field

$$\Theta(t) = \Theta_b + \Theta_s \sin(2\pi f t) \tag{11}$$

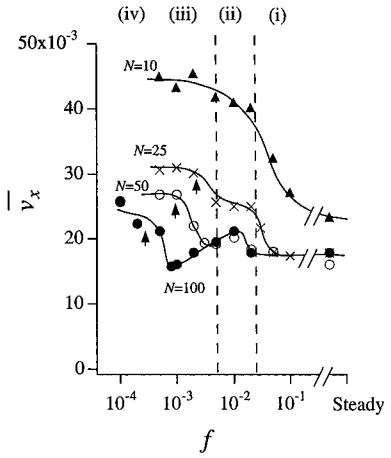

Figure 3. The average migration velocity $\overline{v_x}$. Solid lines are drawn to guide the eyes.

where Θ_b and Θ_s are fixed at $\Theta_b = 0.1$ and $\Theta_s = 0.3$ and f was varied from 10^{-4} to 10^{-1}.

The unit of length corresponds to the Kuhn length of the double strand DNA and is about 120 nm (360 bp).[18] For $q = 720e \times 0.17$,[19] $T = 300$ K, and $a = 120$ nm, 1 V/cm corresponds to $\Theta \simeq 0.04$.

Gel concentration is represented by the number of obstacles C per the area of a^2. Since the radius of the obstacle is $0.25a$, the average pore size ξ can be estimated by

$$\xi = (C^{-1/2} - 2 \times 0.25)a \tag{12}$$

We took $C = 0.5$, which gives $\xi \simeq 0.9a$. This corresponds to agarose gel of 1 wt %, where the average pore size is about 100 nm.[1]

The chain length was varied as $N = 10$, 25, 50, 100, which corresponds to contour length 1.2, 3, 6, 12 μm or to molecular weight 3.6, 9, 18, 36 kbp. Continuous calculation was done more than 80 000 time steps for $N = 10$, 25, 50, and 60 000 time steps for $N = 100$. The calculation time step was fixed at $\delta t = 0.002\zeta a^2/k_BT$.

2.4. Simulation Procedure. Simulation Cell. The size of the simulation cell was $300a$ along the field direction and $100a$ along the direction perpendicular to it. We employed the periodic boundary condition in both direction.

Generation of the Obstacles. The centers of the obstacles were placed randomly in the simulation cell. Therefore the obstacles may overlap. The location of the obstacles was the same under all conditions in the present simulation.

Initial Conformation. An equilibrium conformation of the chain in the field U^{gel} was used as the initial conformation of the chain.

Data Acquisition. The simulation was done over 60 000 time steps for $N = 100$. For other N, it was over 80 000 time steps. To eliminate the effect of the initial configuration, we performed data acquisition after 10 000 time steps.

3. Results

3.1. Averaged Values. Velocity. Figure 3 shows the average center of mass velocity, $\overline{v_x}$, plotted against the frequency of the applied field, f, for various chain length, N. Here x is the direction of the applied field and $\overline{v_x}$ is obtained by

$$\overline{v_x} = \frac{r_{gx}(t=t_l) - r_{gx}(t=t_f)}{t_l - t_f} \tag{13}$$

where $r_{gx}(t)$ is the x component of the position vector of the center of mass:

$$r_{gx}(t) = \frac{1}{N}\sum_i^N r_{ix} \tag{14}$$

t_f is the first time at which the data acquisition starts, and t_l is the last time at which the data acquisition ends.

It is seen that the frequency dependence of the velocity is in good agreement with the experiment of Shikata et al.[6] For the shortest chain of $N = 10$, the velocity $\overline{v_x}$ changes from the high-frequency limiting value to the low-frequency one at about $f \simeq 2 \times 10^{-3}$. For $N = 25$, a plateau-like region appears for $2 \times 10^{-3} < f < 5 \times 10^{-1}$. For $N = 50$, the velocity shows a local maximum at $f \simeq 10^{-2}$ and a minimum at $f \simeq 5 \times 10^{-3}$, the latter corresponding to the antiresonance phenomenon. The chain of $N = 100$ indicates more clearly the antiresonance phenomenon.

The longer chains of $N = 50$ and 100 show a local maximum which is independent of the chain length. This is also consistent with the experiment. Shikata et al.[6] suggested that the local maximum (and the increase of the velocity with the decrease of the frequency) is caused by some elastic response of the gel. However, since the present simulation which uses fixed obstacles shows the same results, we think that the local maximum is due to an intrinsic internal motion of the chain. A possible mechanism for this will be discussed later.

Conformation. To investigate the conformational change of the chain quantitatively, we calculated $R_l(t)$, which stands for the larger principal value of the radius of gyration tensor; i.e,

$$R_l^2(t) = \frac{1}{2}(S_{xx} + S_{yy}) + \frac{1}{2}[(S_{xx} - S_{yy})^2 + 4S_{xy}^2]^{1/2} \tag{15}$$

where $S_{\alpha\beta}$ represents the radius of gyration tensor defined by

$$S_{xx}(t) = \frac{1}{N}\sum_i^N (r_{ix} - r_{gx})^2 \tag{16}$$

$$S_{yy}(t) = \frac{1}{N}\sum_i^N (r_{iy} - r_{gy})^2 \tag{17}$$

$$S_{xy}(t) = \frac{1}{N}\sum_i^N (r_{ix} - r_{gx})(r_{iy} - r_{gy}) = \frac{1}{N}\sum_i^N r_{iy} \tag{18}$$

The chain of a completely stretched linear conformation gives $R_l^2 = N^2a^2/12$, while the chain of an isotropic coiled conformation gives $R_l^2 = Na^2/12$.

Figure 4 shows the average values of $R_l(t)$ under each condition. For comparison, $\overline{v_x}$ values are also plotted. It is seen that $\overline{R_l}$ behaves quite differently from $\overline{v_x}$. For $N = 10$, $\overline{R_l}$ is almost independent of f, while $\overline{v_x}$ decreases by a factor of $1/2$ as the frequency f increases. For $N = 25$ and 50, $\overline{R_l}$ changes from the low-frequency limiting value to the high-frequency limiting value in $10^{-3} < f < 5 \times 10^{-2}$. On the other hand, $\overline{v_x}$ changes its value, showing the minimum and the maximum. For

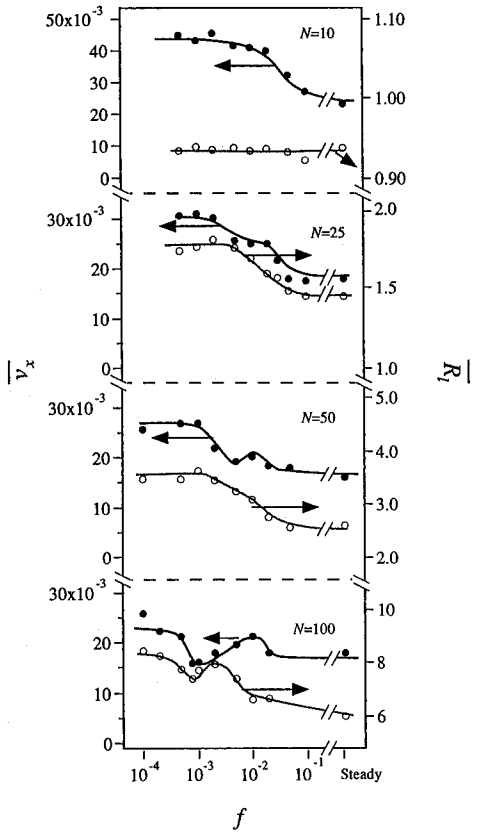

Figure 4. The average value of the larger principal values of the gyration tensor $\overline{R_1}$. Lines are to guide the eyes.

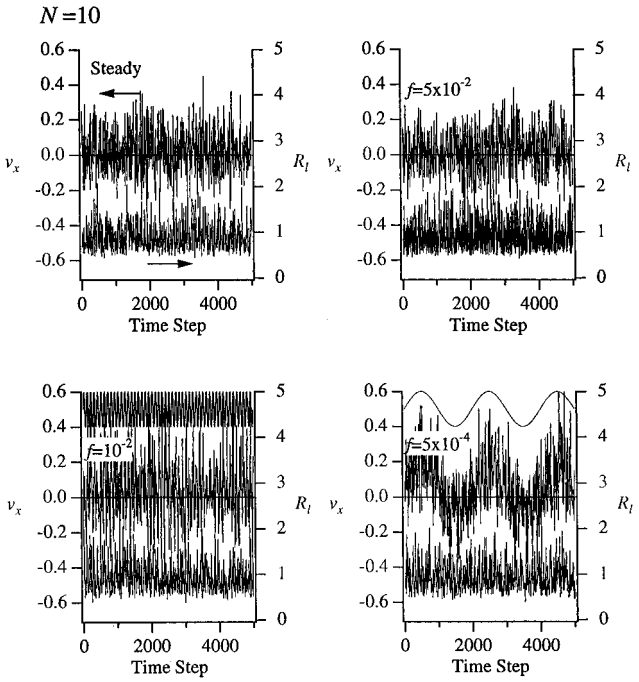

Figure 5. Time development of v_x and R_1 for $N = 10$.

$N = 100$, $\overline{R_1}$ shows a local minimum at the same frequency as the velocity does. $\overline{R_1}$ also shows a local maximum at the frequency which is different from the frequency corresponding to the local maximum of $\overline{v_x}$.

3.2. Time Development. Figures 5 and 6 show an example of the time evolution of $v_x(t)$ and $R_1(t)$ for each condition. $v_x(t)$ was calculated by the Savitzky−Golay method:[20]

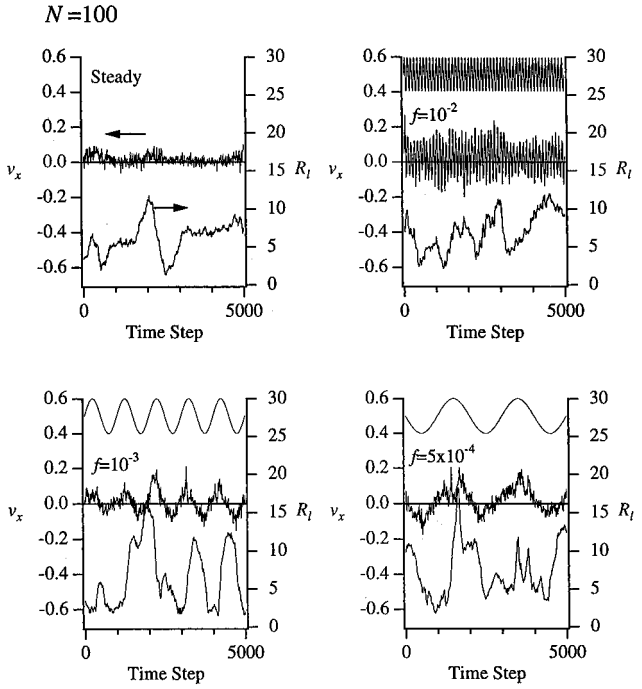

Figure 6. Time development of v_x and R_1 for $N = 100$.

$$v_x(t) = \frac{1}{60\Delta t}\sum_{i=1}^{4} i r_{gx}(t + i\Delta t) - i r_{gx}(t - i\Delta t) \quad (19)$$

where Δt was taken to be one time step under all conditions except for the case of $N = 100$ and $f < 2 \times 10^{-2}$, where Δt was taken to be two time steps. For comparison, the time variation of the field is also plotted in each figure.

It is seen that the velocity of the center of mass $v_x(t)$ follows the field even for the highest frequency. On the other hand, the characteristic features of $R_1(t)$ vary depending on the chain length N.

For $N = 10$, the behavior of $R_1(t)$ for each frequency looks similar to each other. As it is indicated in Figure 4, the average value of $R_1(t)$ is independent of f. Also the magnitude of fluctuations and the relaxation time seem to be independent of f.

For $N = 100$, $R_1(t)$ shows large fluctuations which are not directly correlated to the applied field. The large fluctuation of $R_1(t)$ corresponds to the stretch−contract motion: the chain migrates, taking a stretched conformation and a crumpled conformation alternatively. The fluctuations become larger and more frequent as the frequency f decreases. Also the amplitude of the fluctuations of $R_1(t)$ varies with the field strength $|\Theta(t)|$ at low frequency.

To demonstrate the difference in the behavior of $v_x(t)$ and $R_1(t)$, we calculated the autocorrelation functions $C_{aa}(t)$ as

$$C_{aa}(t) \equiv \frac{\int_0^{t_e}(a(t' + t) - \bar{a})(a(t') - \bar{a})\,dt'}{\int_0^{t_e}(a(t') - \bar{a})^2\,dt'} \simeq \frac{\sum_{i=0}^{t_e}(a(t_i + t) - \bar{a})(a(t_i) - \bar{a})}{\sum_{i=0}^{t_e}(a(t_i) - \bar{a})^2} \quad (20)$$

where $a(t)$ stands for $v_x(t)$ or $R_1(t)$. Figure 7 shows the

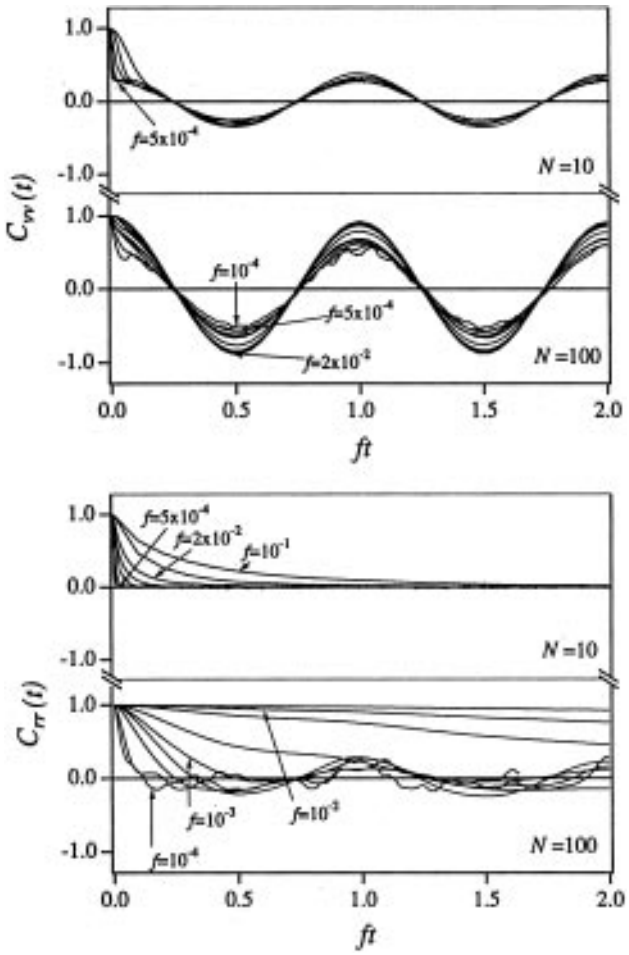

Figure 7. Autocorrelation functions of $v_x(t)$ and $R_l(t)$ for N = 10 and 100.

autocorrelation functions for $v_x(t)$ and $R_l(t)$ plotted against the scaled time ft. The velocity autocorrelation C_{vv} oscillates with the frequency f. This is consistent with the observation that the velocity varies responding to the applied field. On the other hand, the autocorrelation function of $R_l(t)$ decays with the characteristic relaxation time independent of the frequency f, indicating that the conformational changes is governed by a much slower dynamics of the chain.

3.3. Kink Motion. To characterize the chain conformation in more detail, we analyzed the time development of the kink distribution along the chain. For a given conformation of the chain, we find the bead $i$across which the component of the bond vector $\boldsymbol{u}_i = \boldsymbol{r}_{i+1} - \boldsymbol{r}_i$ changes the sign, i.e. we pick up the i at which $u_i^x u_{i-1}^x < 0$. We call such a point a kink. We then represent the position of the kinks in a one-dimensional coordinate $x = i/N$. Figure 8 shows the time evolution of the distribution of the kinks along the chain.

As it is seen in Figure 8, the kink density is high near the chain ends. This is because the tension near the ends is low, and the chain tends to be crumpled near the ends. On the other hand, the kink density in the middle of the chain shows large fluctuations. This corresponds to the stretch−contraction motion. When the chain is in the contracted state, the kink density is uniform along the chain. When the chain is stretched, the kink density in the middle of the chain becomes very low. In such a region of sparse kinks, one can often see a single kink moving along the chain. This kink corresponds to the apex of the V-conformation (see Figure 9). We call such a kink a "dominant kink",

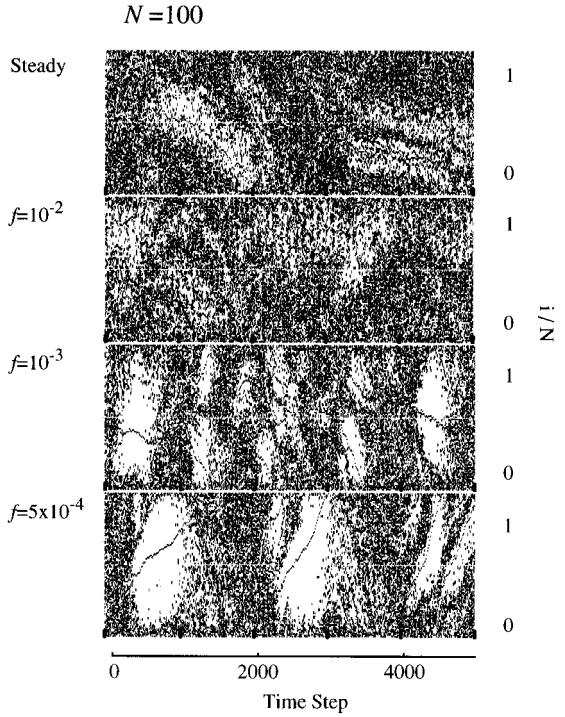

Figure 8. The kink motion in $N = 100$. The origin of the time step is the same for Figure 6.

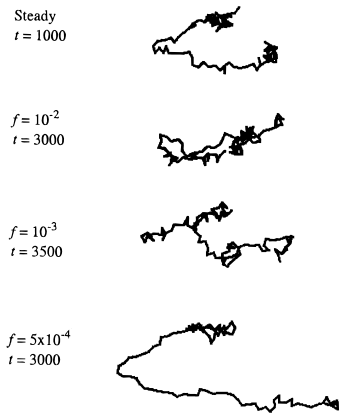

Figure 9. Examples of a snapshot for each condition. The indicated time step corresponds to Figures 6 and 8.

because the stretch−contraction motion of DNA is essentially dominated by such kinks.[21−23]

In BSFGE, the kink motion is affected by the field. At the lowest frequency ($f = 5 \times 10^{-4}$), the sparse region of the kinks appears with the same periodicity as that of the applied field. In the sparse region one can see the dominant kinks running through the chain. Near the antiresonance condition, for $f = 10^{-3}$, the sparse regions are seen periodically. In this case, one can see two or more dominant kinks on the chain. The two dominant kinks correspond to the two apexes of the N-conformation, and the three dominant kinks correspond to the three apexes of the W-conformation.

4. Discussion

4.1. Frequency Dependence of the Stretched Stage. During the migration, the chain takes a stretched and a compact conformation alternatively. As shown in Figure 8, it is observed that the stretched conformation is strongly affected by the field modulation, while the compact one is not. To quantify this, we picked up the peaks and the bottoms of $R_l(t)$. R_l^p represents the

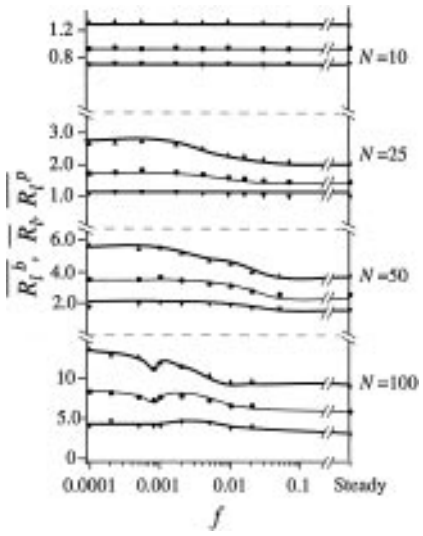

Figure 10. The average extension of the stretched state, $\overline{R_l^p}$, and that of the shrinking state, $\overline{R_l^b}$, plotted against f for various N. For comparison, the average extension, $\overline{R_l}$ is also plotted.

peak which corresponds to the stretched conformation and R_l^b represents the bottom which corresponds to the compact one. The average of R_l^p and R_l^b are plotted against the field frequency f for each N in Figure 10. It is seen that $\overline{R_l^b}$ is almost independent of f. On the other hand, $\overline{R_l^p}$ is strongly dependent on f and its behavior is similar to that of $\overline{R_l}$. This indicates that it is the stretched conformation which is affected by the field modulation.

If we focus on the chain conformation in the stretched stage, we can have a simple picture about the frequency dependence of the chain conformation. We consider the conformation of the chain which is migrating upward. At very high frequency, the stretched conformation is the V-conformation as it is in the steady field. The average velocity and the average elongation are the same as in the steady field without the sinusoidal part (see Figure 4). At very low frequency, the stretched conformation is again the V-conformation, but the direction of the "V" changes alternatively as the field direction changes. The stretched conformation at the intermediate frequency is something between these two limits. As we mentioned in section 3.3, we think that the typical stretched conformation at the antiresonance condition is the W-conformation. In such a configuration, the chain has one hernia and two arms of comparable size. These compete with each other and hinder the chain slipping off the obstacles. We conjecture that this causes the antiresonance phenomenon.

4.2. Modulation Length. To quantify the effect of the field on the conformation, we calculated the mean distance d that each segment migrates during the period for which the field is negative:

$$d = \frac{1}{N}\sum_i \left\langle r_{ix}\left(t=\frac{1}{2\pi f}(2\pi n-\alpha)\right) - r_{ix}\left(t=\frac{1}{2\pi f}(2\pi n-\pi+\alpha)\right)\right\rangle_n$$
$$= \left\langle r_{gx}\left(t=\frac{1}{2\pi f}(2\pi n-\alpha)\right) - r_{gx}\left(t=\frac{1}{2\pi f}(2\pi n-\pi+\alpha)\right)\right\rangle_n$$
$$= \frac{\pi-2\alpha}{2\pi f}\overline{v_x^{\text{inv}}} \qquad (21)$$

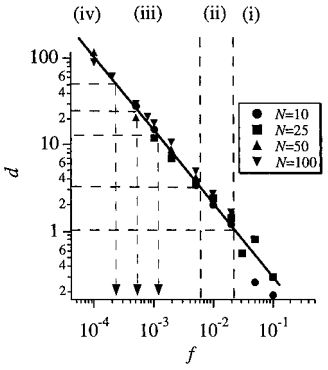

Figure 11. The modulation length d plotted against f.

where $\overline{v_x^{\text{inv}}}$ is the average migration velocity during $\Theta(t) < 0$ and $\alpha = |\arcsin(\Theta_b/\Theta_s)|$. Notice that d is equal to the averaged migration distance of the center of mass during $\Theta(t) < 0$. We call this distance the "modulation length". Figure 11 shows d plotted against f. It is seen that d is dependent on f as $d \simeq f^{-0.9}$ but it is almost independent of N.

4.3. Picture of the Chain Dynamics. Using the modulation length d, we construct a picture of the chain dynamics, and explain the behavior of $\overline{v_x}$ shown in Figure 3.

Region i: $d < 1$. The modulation length is smaller than the Kuhn length of the chain, i.e, than the minimum size of the hernia on the chain. In such a situation, the kink motion is not affected by the field. The motion is almost the same as in the steady field. According to Figure 11, the region of $d < 1$corresponds to the frequency region $f > 2 \times 10^{-2}$. In this region, the migration velocity is close to the steady field value (see Figure 3). The characteristic conformation in this region is the V-conformation, the same as it is in the steady field.

Region ii: $1 < d < d_c$. When d becomes larger than 1, the V-conformation is affected by the field. There are two possible effect of the field modulation: (i) it loosens the apex of the V-conformation and decreases the repulsive force between the chain and the obstacle at the apex of the V-conformation and (ii) it creates many hernias on the arm of the V-conformation and increases the repulsive force between the chain and the obstacles. These effects compete each other. Notice that, at high frequency, the first effect dominates since the created hernias are small and will evaporate due to thermal agitation. For the second effect to be important, the frequency must be smaller than a critical value, f_c. The critical frequency f_c is estimated as follows: We assume that the size of the created hernia is equal to the modulation length d. Since the number of segment included in the hernia of size d is $2d$, the electrical potential of the hernia is $2d\Theta$. Then, the average potential of the hernia during $\Theta(t) < 0$is obtained by

$$U^{\text{hernia}}/k_BT = 2d\frac{(\pi-2\alpha)}{2\pi}\int_{\Theta<0} dt[\Theta_b + \Theta_s \sin 2\pi ft] \qquad (22)$$

Substituting $\Theta_b = 0.1$ and $\Theta_s = 0.3$ into the above equation, we obtain $|U^{\text{hernia}}|/k_BT = 0.26d$. The critical hernia size d_c is estimated by $|U^{\text{hernia}}|/k_BT = 1$. This gives $d_c = 3.8$. According to Figure 11, the critical hernia size $d_c = 3.8$ corresponds to the critical frequency $f_c = 5 \times 10^{-3}$, and the region $1 < d < d_c$ corresponds to the frequency region $2 \times 10^{-2} < f < 5 \times 10^{-3}$. This region includes the local maximum of the migration

velocity. We conjecture that this maximum is caused by the competition between the apex loosening and the hernia creation. The characteristic conformation in this region is the loose apex V-conformation.

Region iii: $d_c < d < N/2$. As the frequency decreases below f_c, larger hernias are created, leading to sluggish migration of the chain. In this region the migration velocity decreases with the decrease of the field frequency. This region includes the antiresonance condition.

Antiresonance: $d = N/4$. When $d = N/4$, the hernia size becomes $2d = N/2$. In this case, the chain frequently takes the W-conformation instead of the V-conformation. Since the hernias and the arms compete with each other, the driving force acting on the chain is canceled out. Consequently, the migration velocity becomes extremely low. This gives the antiresonance. The antiresonance frequency is obtained from Figure 11 at which d is equal to $N/4$.

For the short chains, the antiresonance does not occur because the antiresonance frequency is in the region ii, where the thermal agitation is dominant. Therefore, we can estimate the critical chain length for the antiresonance phenomenon to occur as $N_c = 4d_c$. Under our conditions, substituting $d_c = 3.8$, we obtain $N_c \simeq 15$. This is consistent with the result shown in Figure 3 that the antiresonance does not occur for $N = 10$.

Region iv: $d > N/2$. If the frequency is lowered further, the chain motion is essentially the same as it is in the steady field except it moves forward and backward. If the mean migration velocity $V_{ST}(\Theta)$ for the steady field E is known, the velocity for the biased sinusoidal field at the low-frequency limit is obtained by

$$\lim_{f \to 0} V_{BS}(f) = f\int_0^{1/f} V_{ST}(\Theta_b + \Theta_s \sin 2\pi ft)\, dt \quad (23)$$

This value is usually larger than $V_{ST}(\Theta_b)$, since $V_{ST}(\Theta)$ is proportional to Θ^α with $\alpha \simeq 1.5$.[12] The characteristic conformation in this region is the turning V-conformation.

The Boundaries Between the Regions. The boundaries between the regions are obtained from Figure 11 and indicated in Figure 3. The boundary between regions i and ii and that between regions ii and iii are independent of the chain length. These are indicated by the dashed lines in Figure 3. On the other hand, the boundary between regions iii and iv depends on the chain length. Each boundary is indicated by an arrow head in Figure 3.

Comparison with Experiments. Shikata et al.[6] performed BSFGE experiment varying the parameters of the applied field $E(t) = E_b + E_s \sin 2\pi ft$. They reported that the antiresonance frequency f_p depends on the gel density C_{gel}, the chain length N, and the field strength E_b as

$$f_p \propto C_{gel}^{-1} N^{-1} E_b^1 \quad (24)$$

In our result, it has been shown that $d \propto f^{-0.9}$ corresponding to $f_p \propto N^{-1.1}$. This is close to eq 24.

Although the gel density is not varied in our simulation, we can predict the effect using our picture. According to eq 21, the antiresonance frequency is given by

$$f_c = \frac{2(\pi - 2\alpha)\overline{v_x^{inv}}}{\pi L} \quad (25)$$

The larger the gel density is, the smaller $\overline{v_x^{inv}}$ is. Assuming that $\overline{v_x^{inv}}$ is proportional to the average velocity in the steady field,[12] we have $\overline{v_x^{inv}} \propto C_{gel}^{-0.9}$. This corresponds to $f_p \propto C_{gel}^{-0.9}$ and is close to eq 24.

Comparison with Earlier Works. The above picture is consistent with the earlier pictures proposed for FIGE: the antiresonance occurs when the field switching time matches the deformation time of DNA between the "V"- and "Λ"-conformation.[7,8] We suggest that the W-conformation in our picture of the antiresonance appears due to the difference of the applied field. We are examining our picture for FIGE, and the results will be published elsewhere.

5. Conclusion

In this study, we performed Brownian dynamics simulation of the chain during BSFGE using a new potential. The result is in good agreement with experiments. We analyzed the motion of the kinks and constructed a picture of the chain motion using the modulation length d. This picture explains the experimental results and it is consistent with the earlier pictures in FIGE.

Acknowledgment. This study was financially supported by Research Fellowships of the Japan Society for the Promotion of Science for Young Scientists, No. 0785 and No. 0572.

References and Notes

(1) Nordén, B.; Elvingson, C.; Jonsson, M.; Åkerman, B. *Q. Rev. Biophys.* **1992**, *24*, 103. and references therein.
(2) Zimm, B. H.; Levene, S. D. *Q. Rev. Biophys.* **1992**, *25*, 171 and references therein.
(3) Carle, G. F.; Frank, M.; Olson, M. V. *Science* **1986**, *232*, 65.
(4) Heller, C.; Pohl, F. M. *Nucleic Acids Res.* **1989**, *17*, 5989.
(5) Kobayashi, T.; Doi, M.; Makino, Y.; Ogawa, M. *Macromolecules* **1990**, *23*, 4480.
(6) Kotaka, T.; Adachi, S.; Shikata, T. *Electrophoresis* **1993**, *14*, 313.
(7) Zimm, B. H. *J. Chem. Phys.* **1991**, *94*, 2187.
(8) Duke, T. A. J.; Viovy, J. L. *J. Chem. Phys.* **1992**, *96*, 8552.
(9) Schwartz, D. C.; Koval, M. *Nature* **1989**, *338*, 520.
(10) Smith, S. B.; Aldridge, P. K.; Callis, J. B. *Science* **1989**, *243*, 203.
(11) Deutsch, J. M.; Madden, T. L. *J. Chem. Phys.* **1989**, *90*, 2476.
(12) Oana, H.; Masubuchi, Y.; Matsumoto, M.; Doi, M.; Matsuzawa, Y.; Yoshikawa, K. *Macromolecules* **1994**, *27*, 6061.
(13) Åkerman, B. *Electrophoresis* **1996**, *17*, 1027
(14) Lee, N.; Obukhov, S. P.; Rubinstein, M. *Electrophoresis* **1996**, *17*, 1011.
(15) Masubuchi, Y.; Oana, H.; Matsumoto, M.; Doi, M.; Yoshikawa, K. *Electrophoresis* **1996**, *17*, 1065.
(16) Shaffer II, E. O.; Olvera de la Cruz, M. *Macromolecules* **1989**, *22*, 1351.
(17) Matsumoto, M.; Doi, M. *Mol. Sim.* **1994**, *12*, 219.
(18) Yoshikawa, K.; Matsuzawa, Y.; Minagawa, K.; Doi, M.; Matsumoto, M. *Biochem. Biophys. Res. Commun.* **1992**, *188*, 1274.
(19) Schellman, J. A.; Stigter, D. *Biopolymers* **1977**, *16*, 1415.
(20) Savitzky, A.; Golay, M. J. E. *Anal. Chem.* **1964**, *36*, 1627.
(21) Volkmuth, W. D.; Duke, T.; Wu, M. C.; Austin, R. H.; Szabo, A. *Phys. Rev. Lett.* **1994**, *72*, 2117.
(22) Masubuchi, Y.; Oana, H.; Akiyama, T.; Matsumoto, M.; Doi, M. *J. Phys. Soc. Jpn.* **1995**, *64*, 1412.
(23) Sevick, E. M.; Williams, D. R. M. *Phys. Rev. E.* **1994**, *50*, 3357.

MA961273A